PAPER

Check for updates

A novel poly(amidoamine)-modified electrolyte–insulator–semiconductor-based biosensor for label-free detection of ATP

Zhan Qu, † Muhammad Noman Bashir,† Miaomiao Wang,† Yating Chen, Beenish Noureen, Zhiyao Wang, Yage Liu, Liping Du* and Chunsheng Wu *

Adenosine triphosphate (ATP) is crucial for cellular activity. The need for ATP detection in the field of biomedicine is rapidly increasing. Several biosensor-based approaches have been developed as a result of the growing demand for ATP detection. An electrolyte–insulator–semiconductor (EIS) sensor is a type of field-effect device that has the ability to detect surface-potential changes with a specific level of sensitivity. In this study, a label-free ATP detection biosensor based on poly(amidoamine)-modified EIS sensors was developed, in which an ATP-sensitive aptamer (Apt) was utilized as the sensitive element and the EIS sensor was used as the transducer. It is possible to monitor the binding of charged molecules, such as aptamers using EIS sensors in a label-free manner with a straightforward setup. To improve the coupling efficiency of Apt with the EIS sensor, a positively charged polyelectrolyte, *i.e.*, poly (amidoamine) (PAMAM) dendrimers, was utilized to modify the surface of the EIS sensors to attach the negatively charged Apt through electrostatic attraction. The adsorptive binding of Apt and ATP results in a change in the capacitance of the EIS sensor. During the process of surface modification, the electrochemical measurements of capacitance–voltage ($C–V$) curves and constant-capacitance (ConCap) characteristics were utilized as indicators for the corresponding processes of EIS sensor surface modification. The measurement results indicated that this biosensor was able to detect ATP with high sensitivity and good specificity. The detection range of ATP was from 0.1 nM to 100 nM and the detection limit was as low as 0.12 nM. This biosensor has the potential to be utilized in the detection of ATP in the surrounding microenvironment of cells and tissues, with promising prospects for application in the field of biomedicine such as energy and metabolism monitoring of cells and tissues.

Introduction

Adenosine triphosphate (ATP), as the primary energy currency within cellular systems, plays a pivotal role in both medical diagnostics and scientific investigations. ATP serving as the fundamental energy carrier, stands as a crucial biomolecule within living organisms. Its pivotal functions encompass the regulation of cellular metabolism, facilitation of enzymatic reactions, and orchestration of cellular and tissue activities.[1–3] For example, it is an essential molecule for cellular energy processes and plays a critical role in cardiac metabolism, particularly under conditions of heart failure, thereby highlighting its therapeutic significance.[4] The imperative for ATP quantification in cell biology research is increasingly pronounced. Quantifying ATP levels in cells, tissues or organs might be employed to evaluate their viability during transplantation or surgical procedures. This aids in assessing the efficacy of the treatment and predicting possible consequences. An early diagnosis of diseases can be facilitated by the use of a quick and sensitive ATP biosensor, as ATP levels tend to fall in diseased cells. ATP is found in every cell in existence, including bacteria. Utilizing an ATP-specific biosensor could effectively monitor bacterial infections and provide valuable information for making treatment choices. Therefore, the development of fast, very sensitive, and precise analytical techniques for ATP detection is extremely important in the progress of human healthcare.[5–7] The quantification of ATP levels provides invaluable insights for multifaceted purposes.

Numerous analytical methodologies have been employed for ATP detection. However, many of these techniques primarily focus on measuring the steady-state or equilibrium levels of the analyte, rather than monitoring transient fluctuations, especially in regions closely associated with neurogenic release and activity. Various methods, such as spectrophotometry,[8] molecular sieves,[9] luminescence,[10] photoluminescence,[11] and electrochemical techniques utilizing potentiometric and amperometric biosensors are available for measuring

Institute of Medical Engineering, Department of Biophysics, School of Basic Medical Sciences, Health Science Center, Xi'an Jiaotong University, Xi'an, Shaanxi, 710061, China. E-mail: duliping@xjtu.edu.cn; wuchunsheng@xjtu.edu.cn

† These authors contributed equally.

physiologically relevant ATP levels. There have been numerous reports on detecting ATP and its byproducts during the hydrolysis of ATP. Furthermore, the ability to detect PPi, which plays a critical role in various biochemical processes,[12] including DNA replication,[13] energy transduction, and metabolism, has gained importance in cancer research.[14] Fluorescence sensors are commonly used detection techniques for ATP. And polymer dye composite materials, due to their unique advantages and multifunctionality, improve the stability and sensitivity of fluorescence sensors.[15] In recent years, electrochemical aptamer sensors have gradually emerged. Among these, electrochemical biosensors stand out as promising tools for monitoring transient fluctuations in ATP content both *in vivo* and *in vitro*, particularly in close proximity to release sites.

Aptamers have garnered significant attention owing to their exceptional affinity and specificity. Offering advantages over conventional affinity reagents like enzymes and antibodies, aptamers possess attributes such as chemical stability, facile production, and design flexibility. Aptamers, molecular entities recognized for their specific binding affinity towards ATP, are prominently employed in investigative endeavors aimed at ATP detection and differentiation from its precursor molecules, adenosine diphosphate (ADP) and adenosine monophosphate (AMP),[16,17] using various adsorbents like columns,[18] magnetic beads,[19] and nanoparticles.[20] In recent years, there has been a surge in the utilization of aptamer-modified electrodes for the precise identification of ATP and metabolites.[21-23] One notable application is the direct and immediate assessment of ATP produced by astrocyte cells in cultured environments.

Poly(amidoamine) (PAMAM) dendrimers are a class of well-defined, star-shaped synthetic polymers characterized by a branched, three-dimensional structure emanating from a central core. These branches possess a high degree of customizability, allowing for the attachment of various functional groups, including drugs or other molecules of interest.[24] The unique properties of PAMAMs are not only revolutionizing drug delivery but also making significant advancements biosensing technology.[25] Researchers are exploring PAMAMs to develop exceptionally sensitive biosensors that can identify specific disease markers. By attaching capture molecules like antibodies to the dendrimer branches, these biosensors can achieve exceptional target recognition.[26]

EIS sensors are capacitive detectors that are sensitive to ions. They can detect pH levels, ion concentrations, and other vital biological parameters since they are biochemically sensitive capacitors. When protons are released or biomolecules acquire an intrinsic charge during bio-molecular interactions, they cause changes in the gate voltage, which is how they function. Biomolecules can have their polarity changed by concentrating on their isoelectric point.[27-30] Gate voltage shifts as a consequence of this alteration in local surface charge at the semiconductor–insulator contact.[27] Recently, urea, glucose, rheumatoid arthritis, and DNA amplification have been identified using EIS sensors.[31-34] Additionally, sensors for protein kinase C, creatine kinase II, and protein kinase A have been reported.[35,36]

In this study, a label-free ATP detection biosensor based on PAMAM-modified EIS sensors was developed, in which an ATP-sensitive aptamer (Apt) was utilized as the sensitive element and the EIS sensor was used as the transducer. The EIS sensor is a cost-effective and easily manufacturable capacitor that is sensitive to biological substances. It is anticipated that the Apt, which is immobilized through adsorption, will be oriented flatly on the surface of the EIS. The negatively charged amide group will be attracted to the positively charged PAMAM particles. When a layer of polyelectrolyte with a positive charge is present, there will be increased resistance to the transfer of electrons from the solution to the electrode surface.[30] This is due to the presence of more negative charges and the spatial resistance of PAMAM. As a result, there will be an improvement in sensitivity. The capacitance–voltage ($C–V$) and ConCap characteristics were conducted to examine the changes in sensor capacitance resulting from the distinctive interactions between the positively charged PAMAM-modified weak electrolyte. Essentially, the structural alterations of Apt cause alterations in the electrical charge on the sensor surface, leading to changes in the capacitance of the sensor. Consequently, the sensor was capable of detecting ATP by observing alterations in its capacitance values.

Materials and methods

Materials

Sulphuric acid (H_2SO_4) was purchased from Sinopharm Chemical Reagent Shaanxi Co., Ltd, China. Hydrochloric acid (HCl), Hydrofluoric Acid (HF), silane agent, acetone, NaCl, and ethanol were purchased from Solarbio Science and Technology Corporation, China. Isopropyl alcohol was sourced from Shanghai Aladdin Biochemical Technology Co., Ltd, China. Sodium hydroxide (NaOH) and Phosphate Buffered Saline (PBS) were obtained from Aladdin, China. PAMAM 3.0 was procured from Sigma-Aldrich, USA. A 3 M potassium chloride (KCl) solution was prepared in the laboratory using potassium chloride and deionized (DI) water (18.2 MΩ cm). All aqueous preparations were made using deionized ultra-pure water (DI). The remaining compounds did not require further purification as they were all of analytical grade.

ATP was purchased from Shanghai Biomedical Technology Ltd, China. The ATP-sensitive aptamer (Apt) was acquired from Sangon Biotech (Shanghai) Co., Ltd, China. The sequence of the aptamer is 5′-NH₂-ACCTG GGGGA GTATT GCGGA GGAAG GT-3′.

EIS sensor fabrication

The EIS sensor structure (Au–*n*-Si–SiO₂) was typically constructed on a silicon wafer (*n* type, <100>, 10–15 Ωcm). Initially, a 30 nm SiO₂ layer was formed on the silicon wafer through dry oxidation to serve as an insulating layer. Subsequently, hydrogen fluoride (HF) was employed to etch the rear side of the wafer.[26] Following this, a layer of gold was deposited onto the etched side of the sensor to serve as an ohmic contact for the working electrode. The wafer was then cut into small pieces of the required size, and subjected to sequential washing in an ultrasonic bath with acetone, isopropyl alcohol, ethanol, and

deionized water, in that order. Subsequently, the wafer sensor chip was prepared for further experimental use.[37]

Layer-by-layer modification of the EIS sensor

Positively-charged PAMAM dendrimers were employed to modify the EIS sensor surface through layer-by-layer adsorption of PAMAM and the aptamer. This process enhances sensor performance by bringing the target molecules closer to the gate surface within a Debye length, resulting in a stronger sensor signal.[38] The sensor surface is initially prepared by forming a polyelectrolyte layer through activation and cleaning procedures. Subsequently, PAMAM dendrimers are adsorbed onto this modified surface. The aptamer is then immobilized onto the sensor surface, facilitating the highly sensitive and specific detection of target molecules, such as proteins.

The successful formation of the PAMAM dendrimer/aptamer bilayer on the sensor surface can be verified through fluorescence and AFM characterization. So, in this study, the layer-by-layer method involves adsorbing positively charged PAMAM dendrimers onto the negatively charged SiO$_2$ sensor gate insulator surface, followed by immobilizing the Apt onto the already immobilized positively charged PAMAM layer. This layer-by-layer immobilization method often forms elongated structures. Consequently, this investigation used liquids with low ionic strength. ATP molecules could be trapped in close proximity to the gate surface, inside the Debye length, resulting in an increased signal. Then a 1.0 g per L PAMAM solution was utilized to treat the EIS sensor surface for at least 10 minutes allowing for the formation of a polyelectrolyte layer.[39]

A high ionic strength solution of PAMAM was selected (10 mM NaCl) to maximize the adsorption of PAMAM on the surface of the EIS sensor. After the immobilization of PAMAM on the surface, the sensor was subjected to a triple washing operation using a measuring solution in order to remove non-attached or unbound materials from its surface. Subsequently, for the immobilization of the aptamer, 3.0 μL of aptamer solution at a concentration of 100 μM was used to treat the EIS sensing surface that had previously been treated using PAMAM. Prior to conducting the EIS measurement, the EIS sensor with the modified PAMAM/Apt bilayer surface was stored at 4 °C for further experiments.

Characterization of the PAMAM-based EIS sensor

Scanning electron microscopy (SEM) and the atomic force microscopy (AFM) were used to characterize the adsorption of PAMAM onto the surface of the EIS sensor. For this, four samples were constructed for characterization: a standard bare EIS sensor, an EIS sensor modified with PAMAM, an EIS sensor modified with PAMAM/Apt, and an EIS sensor modified with PAMAM/Apt/Atp. The samples were prepared for SEM analysis by mounting them on stubs and applying a 10 nm gold sputter coating. The samples were analyzed using a SEM (GeminiSEM 500, Zeiss, Germany) at an accelerating voltage of 5 kV. For AFM characterization, the samples were imaged (2 μm × 2 μm) using a scanning probe microscope (SPM-9700HT, SHIMASZU, Kyoto,

Japan) in tapping mode with gold-coated cantilevers (scan speed: 1 Hz).

Fluorescence microscopy was employed to validate that the aptamer had successfully attached onto the surface of the polyelectrolyte-modified SiO$_2$. For this, the Apt was labelled with FAM, which is a green fluorescent label. The samples were observed and imaged under a fluorescent microscope (Axio Imager Al m, Zeiss, Germany).

Electrochemical measurements

For electrochemical measurements, an electrochemical workstation (Zennium, Zahner. Elektrik, Bad. Staffelstein, Germany) was employed. As shown in Fig. 1, the measurement system comprised three electrodes: a Pt wire (counter. electrode), Ag/AgCl (reference electrode), and EIS sensor (working electrode). The measurement solution used was a low-ionic strength NaCl solution with a concentration of 10 mM and a pH of 5.45. The EIS sensor, designed to detect ATP, was placed within a measurement chamber that had been developed at home. The chamber consisted of an EIS surface, a plastic holding box with a square aperture at the bottom, and a silicon rubber sealing ring. The analysis of changes in capacitance values was conducted *via* C–V and constant capacitance measurements. The C–V curves were measured using a low amplitude alternating current voltage (20 mV, 60 Hz) and a direct-current gate voltage ranging from −0.5 V to +1.5 V with increments of 100 mV.

The ConCap measurement was conducted using a feedback control circuit and a predetermined capacitance calculated from C–V measurements, followed by the application of a gate voltage. In order to reduce the impact of both ambient lighting and electromagnetic fields, a Faraday cage was used to protect the whole measuring chamber throughout the experiment. The results obtained from the electrochemical experiments were evaluated using the Origin 9.9 pro program.

Results and discussion

Characterization of EIS sensor surface modification

PAMAMs have been used in the creation of exceptionally responsive biosensors capable of identifying certain target
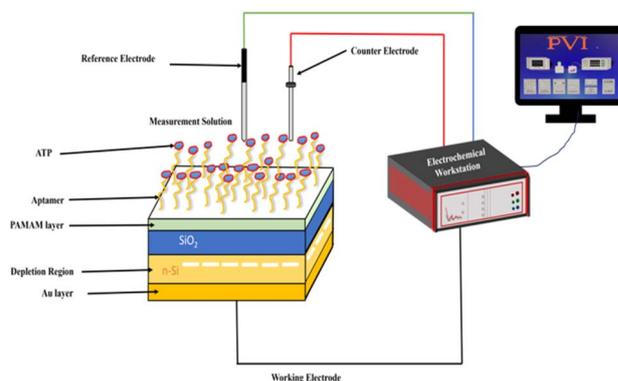

Fig. 1 Schematic diagram of a PAMAM-modified aptamer-based EIS sensor for ATP detection.

molecules, highlighting the expanding role of PAMAMs in biosensing technology. As a result, we can expect that the PAMAM-modified EIS sensor has the potential to enhance the coupling effectiveness of the Apt alongside the EIS sensor, hence improving the performance of the Apt-based EIS sensor for ATP detection.

The physical structure of the EIS sensor surface was characterized using SEM after the absorption of PAMAM and the immobilizing effect of the Apt on the sensor's surface. Fig. 2 shows the typical SEM images of EIS sensor surfaces modified with different materials, which include the bare EIS sensor surface, the EIS sensor surface modified with PAMAM attachment, and the EIS sensor surface modified with PAMAM/Apt attachment, and the EIS sensor surface modified with PAMAM/Apt/ATP attachment. The bare EIS sensor can be seen in Fig. 2(a) showing no attachment on the surface of the electrode. As seen in Fig. 2(b), after the immobilization of PAMAM dendrimers on the surface of the bare electrode, the SEM image of the PAMAM-modified EIS sensor surface clearly shows that PAMAM dendrimers were successfully attached on the surface give a white bead-like or white dot-like appearance on the surface. The formation of a white spherical dot is due to the immobilization of PAMAM dendrimers on a bare SiO_2 sensor surface. The PAMAM dendrimers are represented as white dots on the SiO_2 surface. In addition, the PAMAM-modified surface shown in Fig. 2(b) indicates that the spreading of PAMAM particles on the EIS sensor surface is uniform and the PAMAM dendrimers have formed aggregates, exhibiting cluster structures. The size of PAMAM clusters varies between 125 nm and 290 nm.

Once PAMAM is immobilized on the EIS sensor surface, the Apt is then attached to the surface to form a composite of PAMAM and Apt. When the Apt is immobilized on the PAMAM modified electrode surface, it modifies the structure of the surface of the electrode. Following the placement of Apt onto the SiO_2 surface, modifications to the morphology of the surface

of the EIS sensor were observed. This led to the creation of a dense structure on the PAMAM modified sensor that was more closely packed than the PAMAM layer that was used alone. The modification of the surface of the EIS sensor can be clearly seen in Fig. 2(c). It shows that the attachment of Apt on the PAMAM-modified EIS sensor surface forms some more cluster-like structures on the EIS electrode surface, which increase surface roughness. Moreover, it seems that PAMAM/Apt covering the sensor surface shows more bead-like white structures on the surface.

Fig. 2(d) clearly shows the ATP molecules attached on the PAMAM/Apt-modified surface. The size of the beads increases compared to the previous ones proving that ATP molecules are successfully attached to the aptamer. The size of bead-like structures ranges from 300 nm to 500 nm. The SEM characterization results revealed that the complex structure of chemicals is tightly bound to the EIS sensor surface. The SiO_2 surface coated with a PAMAM/Apt composite was fixed with Apt, modifying the composition of the EIS sensor interface. Following the immobilization of the Apt, the morphology of the sensor undergoes additional significant alterations when ATP molecules are immobilized on the surface that has been modified with the aptamer. Due to the binding of ATP molecules with the aptamer, which is sensitive to ATP, the structure appeared to be more compact and denser. This indicated that ATP molecules are successfully attached to the aptamer.

The sensor's surface roughness was further characterized by AFM height pictures using the Root Mean Square (RMS) method, measuring the variations in the surface area. Fig. 3 displays typical AFM images of the surface of a bare EIS sensor and after modification with PAMAM, Apt, and ATP. The two dimensional and three-dimensional pictures of the bare SiO_2 sensor surface can be seen in Fig. 3. The surface of the bare EIS sensor is clear showing no chemical attachment on the surface. Therefore, the surface roughness shows an average root mean square value of only 1.37 nm. The EIS sensor surface after PAMAM absorption changes its morphology due to the attachment of the PAMAM layer on the surface. Therefore, the roughness of the surface also changes. The difference in roughness can be seen by comparing it with the bare electrode
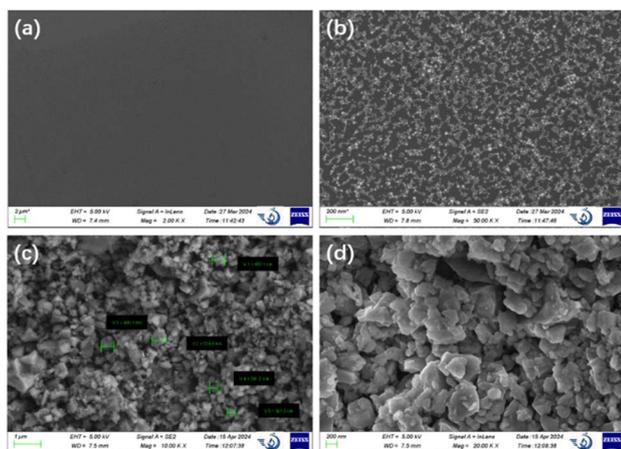

Fig. 2 Typical images of SEM characterization of (a) bare EIS sensor surface, (b) EIS sensor surface modified with PAMAM, (c) EIS sensor surface modified with PAMAM/Apt, and (d) EIS sensor surface modified with PAMAM/Apt/ATP.
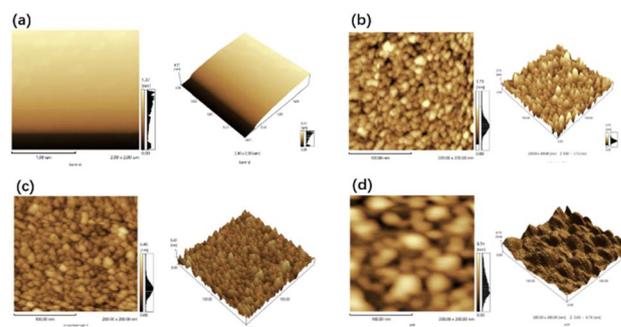

Fig. 3 Typical images of AFM characterization of (a) bare EIS sensor surface, (b) EIS sensor surface modified with PAMAM, (c) EIS sensor surface modified with PAMAM/Apt, and (d) EIS sensor surface modified with PAMAM/Apt/ATP.

surface. Upon the adsorptive immobilization of the PAMAM molecule, the surface roughness increases to 3.73 nm (Fig. 3(b)). The AFM images of the PAMAM layer obtained from various regions of the EIS sensor surface indicate that the PAMAM is uniformly spread over the surface, indicating that the PAMAM particles are oriented in a flat manner. Furthermore, the AFM image reveals several dense and extremely porous nanofilms, indicating an even distribution of PAMAM on the SiO_2 surface. The AFM images reveal a high concentration of dendrimer aggregates on the surface, which is similar to the PAMAM/SWNT layer-by-layer films that were recently described on a silicon surface with varying numbers of bilayers.[39] Due to the varying sizes of AFM tips employed, it is not feasible to determine whether the dot-shaped nanostructures are present on the light PAMAM layer situated on the SiO_2 layer or directly on the SiO_2 layer.

The AFM images reveal substantial changes in the surface microstructure of the SiO_2 layer following the addition of PAMAM and Apt. As shown in Fig. 3(c), the surface structure underwent dramatic changes after immobilizing the Apt on the PAMAM-modified silicon dioxide EIS sensor surface. The PAMAM/Apt bilayer is covered with large clusters, resulting in an increase in surface roughness to 6.40 nm. The AFM characterisation findings validate the successful formation of a bilayer consisting of PAMAM and Apt on the surface of the EIS sensor. The presence of bead-like structures on the surface indicates a uniform distribution of PAMAM/Apt, as observed in Fig. 3(c). The surface morphology continues to change after the immobilization of ATP on the PAMAM/Apt modified SiO_2 surface, as observed in Fig. 3(d). These changes also cause changes in the roughness of the surface. The roughness of the surface increases to 9.74 nm. These characterization results also verify the successful attachment of ATP on the PAMAM/Apt bilayer surface. Clusters of materials and tiny yellow molecules show the attachment of ATP with aptamer molecules which are sensitive to the ATP molecules.

Fluorescence spectroscopy was used to validate the immobilization of the Apt. The Apt, labelled with FAM, was used to confirm the effective immobilization of the Apt on the PAMAM layer. The process was validated by first adding a FAM-labelled Apt to the exterior of a PAMAM-modified EIS biosensor. Fig. 4 showed the results of fluorescence measurements when exposing the surface of the EIS sensor coated with PAMAM to a solution containing 5 µM of Apt labelled with FAM. Furthermore, it presents the outcomes after the incubation of the EIS sensor, modified with a PAMAM/Apt bilayer, with a 5 µM ATP solution. The bare EIS biosensor did not exhibit any fluorescence signal upon exposure to the FAM-labelled Apt mixture (Fig. 4(a)). The immobilization process is impeded by the electrostatic repulsion that occurs between the negative-charged Apt and SiO_2 surfaces. After the washing operation, no FAM-labelled Apt molecules remain on the uncoated EIS sensor surface. After the PAMAM-modified EIS sensor substrate was incubated with the FAM-labelled Apt mixture, as shown in Fig. 4(b), a robust and consistent fluorescence signal was detected, demonstrating the successful attachment of Apt molecules to the positively charged PAMAM layer. The
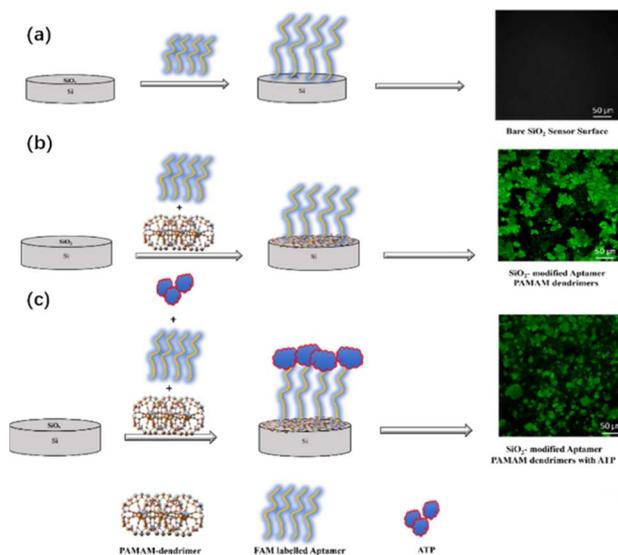

Fig. 4 (a) Fluorescence image of the bare EIS sensor surface with the FAM-labelled Apt and without the PAMAM dendrimer layer. (b) Fluorescence image of the EIS sensor surface with the FAM-labelled Apt and PAMAM dendrimer layer. (c) Fluorescence image of the EIS sensor surface with the FAM-labelled Apt, PAMAM dendrimer layer and ATP.

fluorescence signal remained there after six rinse processes without any reduction in intensity. The PAMAM dendrimer's dendritic structure enables an enhanced attachment of the Apt to the EIS sensor surface. Fig. 4(c) shows a faint fluorescence signal following the binding of ATP with the FAM-labelled Apt, in contrast to Fig. 4(b). The experiment validates the successful immobilization and attachment of the FAM-labelled Apt to the positively charged PAMAM layer.

Label-free detection of ATP

This work focused on detecting ATP without the use of PAMAM-modified EIS biosensors. Changes in potential were detected by ConCap measurements and the measurement of variations in capacitance was conducted using the $C–V$ curves shift mode after the attachment of the PAMAM dendrimer, Apt, and ATP molecules to the surface of the EIS sensor. The changes in the electrochemical measurements were due to conformational modifications in the composition of these compounds adhered to the surface of the EIS sensor. These changes were recorded in each step of the adsorption or immobilization process. The capacitance voltage curves of the bare EIS electrode underwent alterations following the adsorption of the PAMAM dendrimer. Subsequently, after the successful immobilization of the aptamer on the PAMAM-modified surface, and finally following the attachment of ATP molecules on the modified EIS sensor, further modifications in the electrochemical measurements were observed. Specifically, the ConCap measurements and $C–V$ curves of the EIS sensor were initially recorded on the bare sensor in a 10 nM NaCl solution at pH 5.45. Subsequent measurements were conducted after the attachment or adsorption of the dendrimer (PAMAM), followed by the attachment of the aptamer on the PAMAM-modified surface.

Lastly, measurements were performed after the immobilization of ATP molecules on the PAMAM/Apt modified EIS sensor.

The electrochemical measurements, *i.e.*, ConCap measurements and *C*–*V* curves of the EIS sensor, were performed using an EIS sensor immersed in a 10 nM NaCl solution at a pH of 5.45, after the attachment of the PAMAM dendrimer, following the immobilization of the Apt on the PAMAM-modified EIS sensor surface, and finally after the capture of ATP molecules on this PAMAM/Apt-modified EIS sensor. The capacitance in the accumulation region of the *C*–*V* curve remains almost constant until the surface modification stages are finished. Significant changes in the *C*–*V* curves have been observed across the voltage axis in the depletion region. The variations in the direction & amplitude vary based on the sign and magnitude of the absorbed charge. These shifts were recorded through an electrochemical workstation. The presented evidence underscores the role of charged macromolecules' absorption and the interaction between components leads to changes in the potential difference at the interface, which in turn affects both the voltage & capacitance of the EIS biosensor structure.[40]

The enlargement of the depletion layer is caused by the attachment of charged molecules, namely, the positively charged PAMAM particles, to the oppositely charged electrode surface that contains SiO_2. As a result, the growth of the depletion layer causes a reduction in the space-charge capacitance inside the silicon, with the semiconductor's variable space-charge capacitance being affected. These electrochemical modifications in the sensor ultimately lead to a decrease in the sensor's overall capacitance, thereby manifesting significant alterations in *C*–*V* curves towards higher negative potential or gate voltage. The *C*–*V* curves continued to change in value after the attachment of the aptamer and ATP molecules. The *C*–*V* curves shifted toward higher voltage after the attachment of the aptamer and the shift became even more pronounced towards the higher gate voltage, when the ATP molecules were attached to the PAMAM/Apt modified EIS sensor. When ATP binds to the aptamer it acts like a hand fitting into a glove. It induces the aptamer to fold or rearrange itself to create a tighter or more precise fit around the ATP molecules. This conformational change or ATP binding to the aptamer often leads to alterations in the physical and chemical properties along with the electrochemical properties. These changes in structures often serve as a signal for the biosensor. So, these changes can be measured through ConCap and *C*–*V* curves. ConCap measurements are frequently employed to monitor real-time potential shifts resulting from conformational alterations on the EIS surface.

These changes are evident when the blank apt sensor is exposed to a range of 0.1 nM to 100 nM ATP concentrations, as depicted in Fig. 5. The ConCap signal of normalized capacitance increases with increasing ATP concentrations, and a heightened ConCap signal was recorded owing to conformational changes in the EIS surface.

Various ATP concentrations, varying from 0.1 nM to 100 nM, were used in ATP detection through the PAMAM-modified EIS sensor. It is indicated that the *C*–*V* curves show a displacement in the depletion zone when varying amounts of ATP are used. The obtained curve shifted to the positive direction after the
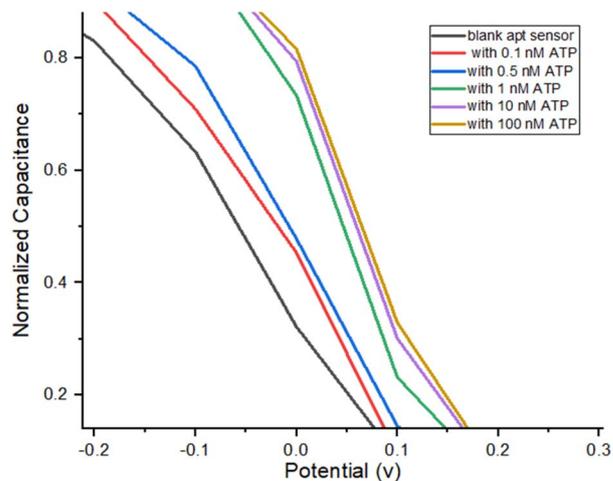

Fig. 5 *C*–*V* measurements of the EIS sensor in response to ATP at different concentrations ranging from 0.1 nM to 100 nM.
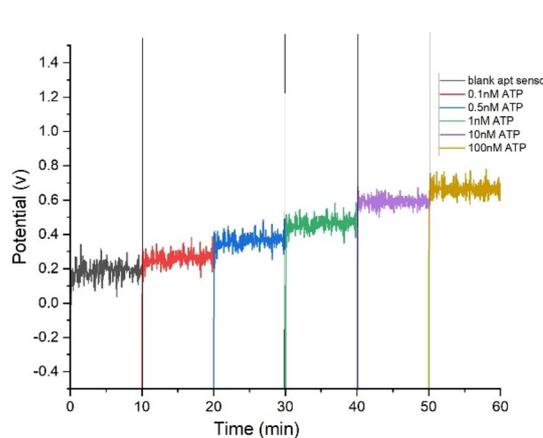

Fig. 6 ConCap measurement of the PAMAM-modified EIS sensor in response to ATP at concentrations ranging from 0.1 nM to 100 nM.
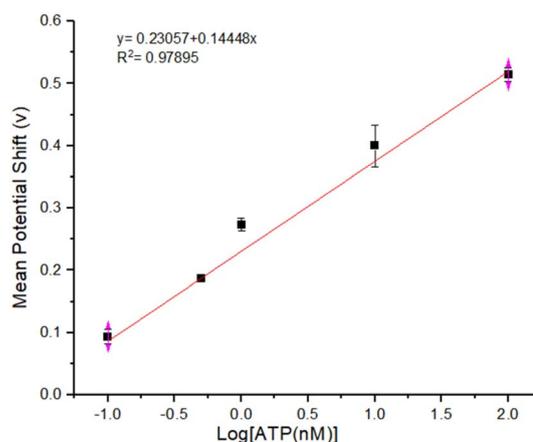

Fig. 7 Statistical results of ConCap measurement for ATP detection on the PAMAM modified EIS sensor in a linear manner. All data are represented as the mean ± SEM, $n = 6$.

ATP attachment ranging from lower to higher ATP concentrations. As shown in Fig. 6, the ConCap signal exhibited a greater potential shift as the concentrations of ATP increased.

A linear and direct correlation was obtained between ATP concentrations and potential changes within the range of 0.1 nM to 100 nM (Fig. 7), which can be represented by the statistical equation: $y = 0.23057 + 0.14448 \times \log[\text{ATP (nM)}]$. While the limit of detection (LOD) of the PAMAM-modified EIS sensor is as low as 0.12 nM. As summarized in Table 1, the performance of this PAMAM-modified EIS sensor for ATP detection is comparable to those of previously reported electrochemical biosensors for ATP detection.[41–45] This PAMAM-modified EIS sensor exhibits superior performance with a lower detection limit and a broader linear range when compared to previously reported electrochemical biosensors.

Three nucleotides, GTP, CTP and UTP, were used to test the selectivity of the PAMAM-modified EIS sensor. The concentrations of these nucleotides were kept higher (100 nM) than that of ATP (10 nM). As shown in Fig. 8, compared with these three nucleotides, the sensor response towards ATP was recorded as very high and significant, showing that this PAMAM-modified ESI sensor has high affinity and good selectivity for ATP. The reason behind this high selectivity is that the aptamer used in this experiment showed no response to the other three nucleotides including GTP, CTP and UTP. But this aptamer has a high response towards ATP even at very low concentrations compared with the concentrations of other nucleotides used. So, these results showed that this biosensor have very high specificity in response to ATP.

In addition, other analytes structurally similar to ATP (*e.g.*, ADP and AMP) were used to further verify the specificity of this biosensor. As shown in Fig. 9, the results indicate that this biosensor has significantly higher signals for ATP (10 nM) than for ADP (100 nM) and AMP (100 nM). All the results suggest strong anti-interference capabilities against ADP and AMP, which further verify the good specificity of this biosensor for ATP detection.

The stability of the prepared PAMAM-modified EIS sensor containing 10 nM of ATP was assessed over a period of 11 days. The PAMAM-modified EIS sensor exhibited high stability for the initial 7 days, after which its responses gradually declined (Fig. 10). Prolonged storage can lead to oxidation, which may cause a decrease in potential shifts. All the results demonstrated that this PAMAM-modified EIS sensor for detection of ATP is very efficient and highly sensitive compared to previously
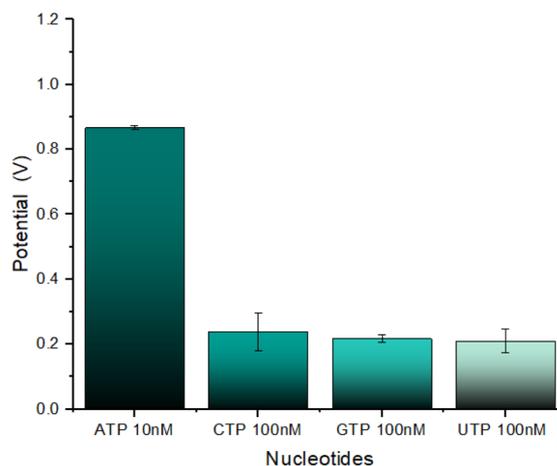

Fig. 8 Results of specificity testing of the PAMAM-modified EIS sensor using 10 nM ATP, 100 nM CTP, 100 nM. The *Y* axis represents the normalized potential shifts. All data are represented as the mean ± SEM, *n* = 5.
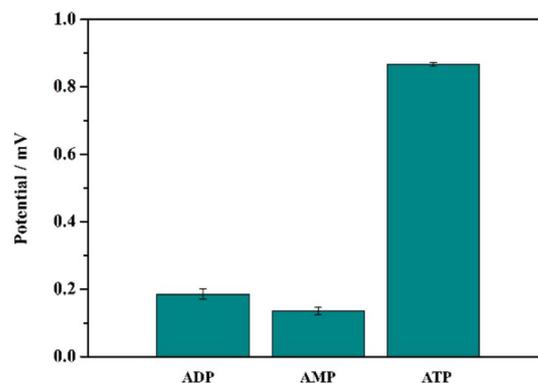

Fig. 9 Specificity testing results of the PAMAM-modified EIS sensors for ATP detection. The *Y* axis represents the normalized potential shifts. All data are represented as the mean ± SEM, *n* = 3.

reported electrochemical biosensors. Additionally, this PAMAM-modified EIS sensor is portable and very easy to prepare and use due to layer-by-layer preparation of the biosensor.

Finally, spiked biological samples were used to demonstrate the practical applicability of this biosensor. Fetal bovine serum was spiked with an ATP standard solution to simulate real

Table 1 Comparison of performances of different ATP sensors

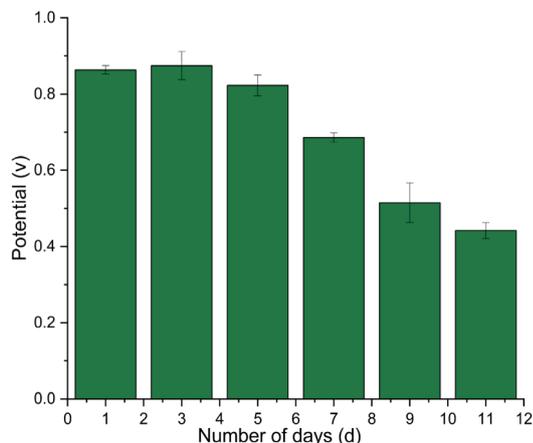| Sensitive materials	Method	Detection limit	Ref.
Gold nanoparticles	Fluorescence	100 nM	41
CHA and dual recycling amplification	Fluorescence	8.2 nM	42
CdSe/CdS/quantum dots	Electrochemiluminescence	3.09 nM	43
ThT-PSS	Fluorescence	3.3 μM	44
GO	Fluorescence	25 μM	45
PAMAM	Electrochemistry	0.12 nM	This work

Fig. 10 Stability testing results of the PAMAM-modified EIS sensors for ATP detection. The *Y* axis represents the normalized potential shifts. All data are represented as the mean ± SEM, *n* = 3.

Table 2 Results of ATP detection in spike samples (*n* = 3)

Sample	Added/nM	Found/nM	Recovery/%
ATP	1	11.17	85.47
	10	10.81	92.50
	100	85.50	117.50

sample detection. The results, presented in Table 2, show a pretty good recovery rate for ATP detection.

Conclusions

This study developed a label-free ATP detection biosensor using PAMAM-modified EIS sensors. A label-free and simple setup can monitor the binding of charged molecules like ssDNA or dsDNA using EIS sensors. The *C*–*V* and ConCap measurements showed that the biosensor detected ATP with high sensitivity and specificity ranging from 0.1 to 100 nM with a limit of detection of 0.12 nM. The performance of this biosensor was stable for 7 days. Based on the EIS structure, a label-free ATP detection method was developed that is simple, inexpensive, and reliable. This biosensor can detect ATP in the microenvironment due to its very high sensitivity and excellent selectivity. The biosensor is pretty simple and cost-effective. It has great potential for detecting ATP without the need for labelling, which is very helpful in the field of biomedicine.

Data availability

The authors confirm that the data supporting the findings of this study are available within the article.

Author contributions

Zhan Qu: conceptualization, methodology, formal analysis, investigation, writing. Muhammad Noman Bashir: conceptualization, methodology, investigation, formal analysis. Miaomiao Wang: methodology, resources, data curation. Yating Chen: investigation, resources, data curation. Beenish Noureen: investigation, data curation. Zhiyao Wang: data curation. Yage Liu: investigation. Liping Du: investigation, methodology, reviewing and editing. Writing – reviewing and editing. Chunsheng Wu: writing – review & editing, supervision, project administration, resources.

Conflicts of interest

There are no conflicts to declare.

Acknowledgements

Notes and references

1 A. Tikhonov and A. Vershubskii, *Photosynth. Res.*, 2020, **146**, 299–329.
2 K. Manoj, *Biochem. Insights*, 2018, **11**, DOI: 10.1177/1178626418818442.
3 N. Singh, S. Naveenkumar, M. Geethika and G. Mugesh, *Angew. Chem. Int. Ed.*, 2021, **60**, 3121–3130.
4 G. Lopaschuk, Q. Karwi, R. Tian, A. Wende and E. Abel, *Circ. Res.*, 2021, **128**, 1487–1513.
5 S. Sivagnanam, P. Mahato and P. Das, *Org. Biomol. Chem.*, 2023, **21**, 3942–3983.
6 Z. Saberi, B. Rezaei and T. Khayamian, *Luminescence*, 2018, **33**, 640–646.
7 H. Chen and Y. Zhang, *Crit. Rev. Biotechnol.*, 2021, **41**, 16–33.
8 C. Li, J. Zhao, K. Cheng, Y. Ge, Q. Wu, Y. Ye, G. Xu, Z. Zhang, W. Zheng, X. Zhang, X. Zhou, G. Pielak and M. Liu, *Annu. Rev. Anal. Chem.*, 2017, **10**, 157–182.
9 G. Morciano, A. Sarti, S. Marchi, S. Missiroli, S. Falzoni, L. Raffaghello, V. Pistoia, C. Giorgi, F. Virgilio and P. Pinton, *Nat. Protoc.*, 2017, **12**, 1542–1562.
10 Z. Zhang, J. Feng, P. Huang, S. Li and F. Wu, *Sens. Actuators, B*, 2019, **298**, 126891.
11 X. Zheng, R. Peng, X. Jiang, Y. Wang, S. Xu, G. Ke, T. Fu, Q. Liu, S. Huan and X. Zhang, *Anal. Chem.*, 2017, **89**, 10941–10947.
12 S. Mondal and N. Dey, *J. Environ. Chem. Eng.*, 2024, **12**, 114412.
13 S. Mondal and N. Dey, *J. Mol. Liq.*, 2024, **398**, 123914.
14 S. Mondal and N. Dey, *ACS Appl. Polym. Mater.*, 2024, **6**, 10242–10253.
15 S. Mondal and N. Dey, *Langmuir*, 2024, **40**, 6163–6171.
16 X. Chen, Y. Feng, H. Chen, Y. Zhang, X. Wang and N. Zhou, *Sensors*, 2022, **22**, 2425.
17 L. Li and M. Li, *Adv. Mater.*, 2024, **36**, e2302972.
18 Y. Ding and J. Liu, *J. Am. Chem. Soc.*, 2023, **145**, 7540–7547.
19 H. Qu, L. Wang, J. Liu and L. Zheng, *ACS Sens.*, 2018, **3**, 2071–2078.

20 Z. Chen, Q. Mou, S. Wu, Y. Xie, K. Salminen and J. Sun, *Anal. Chem.*, 2021, **94**, 1397–1405.

21 M. Santos-Cancel, L. Simpson, J. Leach and R. White, *ACS Chem. Neurosci.*, 2019, **10**, 2070–2079.

22 Y. Jiang, W. Ma, W. Ji, H. Wei and L. Mao, *Analyst*, 2019, **144**, 1711–1717.

23 E. Suaebah, Y. Seshimo, M. Shibata, S. Kono, M. Hasegawa and H. Kawarada, *J. Appl. Phys.*, 2017, **121**, 044506.

24 Q. Xu, C. Wang and D. Wayne Pack, *Curr. Pharmaceut. Des.*, 2010, **16**, 2350–2368.

25 E. Bahadır and M. Sezgintürk, *Talanta*, 2016, **148**, 427–438.

26 F. Garkani NEJAD, H. Beitollahi and I. Sheikhshoaie, *Biosensors*, 2023, **13**, 514.

27 T. Bronder, A. Poghossian, S. Scheja, C. Wu, M. Keusgen, D. Mewes and M. Schöning, *ACS Appl. Mater. Interfaces*, 2015, **7**, 20068–20075.

28 T. Lin, D. Kekuda and C. Chu, *Biosens. Bioelectron.*, 2010, **25**, 2706–2710.

29 B. Noureen, N. Ullah, Y. Tian, L. Du, W. Chen, C. Wu and P. Wang, *Talanta*, 2022, **240**, 120185.

30 N. Ullah, B. Noureen, Y. Tian, L. Du, W. Chen and C. Wu, *Nanomaterials*, 2022, **12**, 1505.

31 Y. Lin, A. PurwidYantrI, J. Luo, C. Chiou, C. Yang, C. Lo, T. Hwang, T. Yen and C. Lai, *Biosens. Bioelectron.*, 2016, **79**, 63–70.

32 T. Pan, T. Lin and C. Chen, *Anal. Chim. Acta*, 2015, **891**, 304–311.

33 E. Al-Khalqi, M. Hamid, N. Al-Hardan, A. Jalar and K. Lim, *Biosens. Bioelectron.*, 2020, **21**, 6234–6240.

34 K. Liu, G. Tian, C. Ko, M. Geissler and T. Veres, *Biomed. Microdevices*, 2020, **22**, 1–18.

35 Y. Pan, J. Liu and F. Qi, *Hum. Genom.*, 2019, **13**, 1–13.

36 Y. Choi, J. Jeong and S. Hong, *ACS Appl. Mater. Interfaces*, 2024, **16**, 2101–2109.

37 K. Larsen, D. Petersen, A. Wilkins, I. Samdal, M. Sandvik, T. Rundberget, D. Goldstone, V. Arcus, P. Hovgaard and F. Rise, *Chem. Res. Toxicol.*, 2007, **20**, 868–875.

38 M. Camões, *Chem. International-Newsmagazine IUPAC*, 2010, **32**, 3–7.

39 J. Siqueira, C. Werner, M. Bäcker, A. Poghossian, V. Zucolotto, O. Oliveira and S. Michael, *J. Phys. Chem. C*, 2009, **113**, 14765–14770.

40 S. Cheng, B. Zheng, D. Yao, S. Kuai, J. Tian, H. Liang and Y. Ding, *Spectrochim. Acta, Part A*, 2018, **204**, 180–187.

41 Y. Yang, J. Huang, X. Yang, K. Quan, H. Wang, L. Ying, N. Xie, M. Ou and K. Wang, *Anal. Chem.*, 2016, **88**, 5981–5987.

42 Y. Peng, D. Li, R. Yuan and Y. Xiang, *Biosens. Bioelectron.*, 2018, **105**, 1–5.

43 G. Jie, J. Yuan and J. Zhang, *Biosens. Bioelectron.*, 2012, **31**, 69–76.

44 V. Singh, S. Pandey and P. Singh, *Dyes Pigments*, 2021, **194**, 109577.

45 X. Chen, Y. Feng, H. Chen, Y. Zhang, X. Wang and N. Zhou, *Sensors*, 2022, **22**, 2425.